

## LIQUID BRIDGE ANALYSIS OF SILICON CRYSTAL GROWTH EXPERIMENTS UNDER MICROGRAVITY

I. MARTINEZ

*ETSI Aeronáuticos, Ciudad Universitaria, 28040-Madrid, Spain*

and

A. EYER \*

*Kristallographisches Institut der Universität, D-7800 Freiburg, Fed. Rep. of Germany*

Received 27 October 1985; manuscript received in final form 20 February 1986

A simplified fluid-mechanical interpretation of a floating zone growth experiment performed aboard Spacelab-1 is given, using the capillary liquid bridge theory. A model is developed to simulate the outer shape of crystals grown from axisymmetric feed rods. Ideas are laid down for a more complete thermal simulation of such processes. These models would help experimenters in crystal growth to predict unstable configurations, avoid bridge disruption and achieve crystals of desired shape.

### 1. Introduction

Crystal growth is the aggregation of otherwise dispersed particles to an already existing solid lattice. This process demands some mobility of the particles, thence the disperse phase is a fluid. Although crystal growth from a gaseous phase is sometimes practiced (vapor growth techniques), as well as crystal growth from a cool liquid (solution growth techniques), the bulk of it is achieved by crystal growth from the melt.

This last technique is further classified according to the configuration of the three-phase contact line where the solid/melt interface meets the surrounding medium, that, although sometimes consisting of a solid wall or a molten salt, it is normally an inert gaseous atmosphere. Besides, three different configurations are usually distinguished: pulling a rod out of a molten bath (Czochralski technique), pulling a rod through a furnace (floating zone technique) or pushing a

cylindrical shape through a dye (the most important of these being edge-defined film-fed growth). The latter, really a variation of the Czochralski method, is the more versatile and is catching the market of semiconductor material production (mainly for solar cells), but the floating zone technique, the one dealt with here, presents the advantage of the melt not being contaminated by the dye or crucible materials.

Container-free floating zone growth is a very common technique to get high purity crystals. The main advantage is that any contamination by the crucible material is avoided. Under gravity conditions, this method is used when the surface tension of the materials suffices to compensate the hydrostatic pressure in the melt. High vapour pressure of at least one of the components might prohibit this method, however.

To establish a floating zone, a relative motion between the sample rod to be processed and the furnace is imposed (fig. 1), causing impurities to be swept to the rod ends by the difference in concentration at the melting and solidification fronts.

\* Now at Fraunhofer-Institut für Solare Energiesysteme, D-7800 Freiburg, Fed. Rep. of Germany

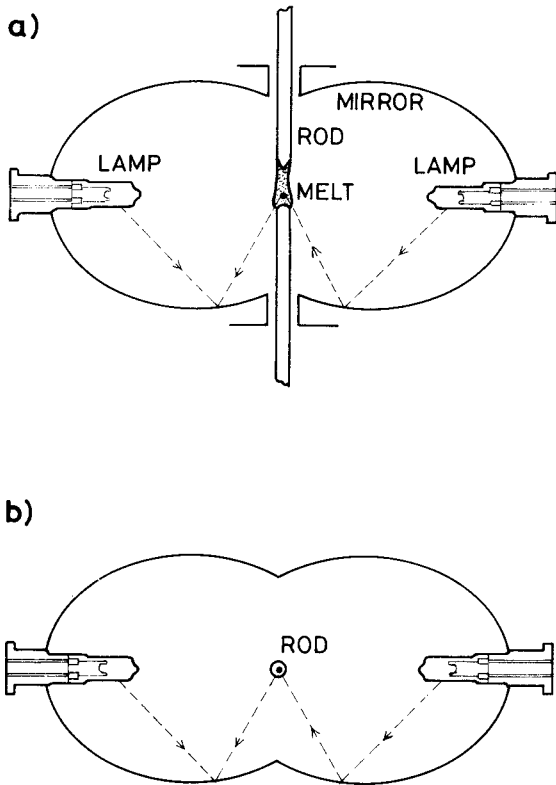


Fig. 1. Double ellipsoidal mirror furnace used in the crystal growth of silicon rods aboard Spacelab-1: (a) side view; (b) plant view.

The interplay of thermodynamical, physico-chemical and fluid-mechanical phenomena in this process is so entangled, that this technology is still full of empirism. Trying to better understand the underlying physics, a great effort is being devoted to the detailed study of more simple specific phenomena, both theoretically and experimentally. In particular, because one of the more conspicuous forces present is that of gravity, a proliferation of microgravity experiments has taken place since the availability of space platforms. Although some of them aim at obtaining new exotic materials, the majority are concerned with more fundamental research, using well known materials, as for instance Experiment 1-ES-312 "Crystal growth of a silicon rod" performed aboard Spacelab-1 in December 1983, which is the one to be analyzed here.

## 2. Growth technique

Two silicon crystals were grown in a so-called Mirror Heating Facility [1], sketched in fig. 1, developed explicitly for zone growth experiments in Spacelab-1, and tested on earth by numerous experiments yielding high quality crystals of different electronic materials (e.g. Si, CdTe, GaSb, InP [2-4]). The radiation of two 400 W halogen lamps is focused on the sample by two adjoint ellipsoidal mirrors. Since the zone is heated by incoherent light, additional forces such as those existing, e.g., in RF heating are avoided. Thus, this method is specially suited to investigate the behaviour of free liquid bridges.

The furnace is moved over the sample, thus making the molten zone travel through prefabricated silicon rods from bottom to top (fig. 2). The special shape shown was chosen to achieve dislocation-free growth by starting the recrystallization in the lower part of the thin neck. A detailed performance description is given in ref. [5]. Fig. 3 shows crystals grown using that furnace.

In such radiation heated silicon growth experiments, the solid/liquid interface at the feed rod (upper interface in fig. 2) tends to be cone-shaped, whereas the growing interface (bottom) is slightly convex [2-6].

Touching of the apex of the cone with the growing crystal has to be avoided in order to maintain monocrystalline structure. Even worse, if both solid ends are being counterrotated, the touching may cause mechanical problems with the drives, and the melt may sputter over the furnace walls. This means that radiation power has to be high enough to exceed a minimal external length of the molten zone. But, on the other hand, an upper limit of this length also has to be attended in order to prevent liquid bridge disruption by capillary forces.

There is a second critical problem aggravating floating zone growth under microgravity conditions. Surek and Chalmers [7] have shown that in silicon the angle between the meniscus of the melt and the growth direction (for constant cross-section growth) has to be  $11^\circ$ , i.e. the molten zone should bulge slightly outward of the growing interface. On the earth, the interaction between

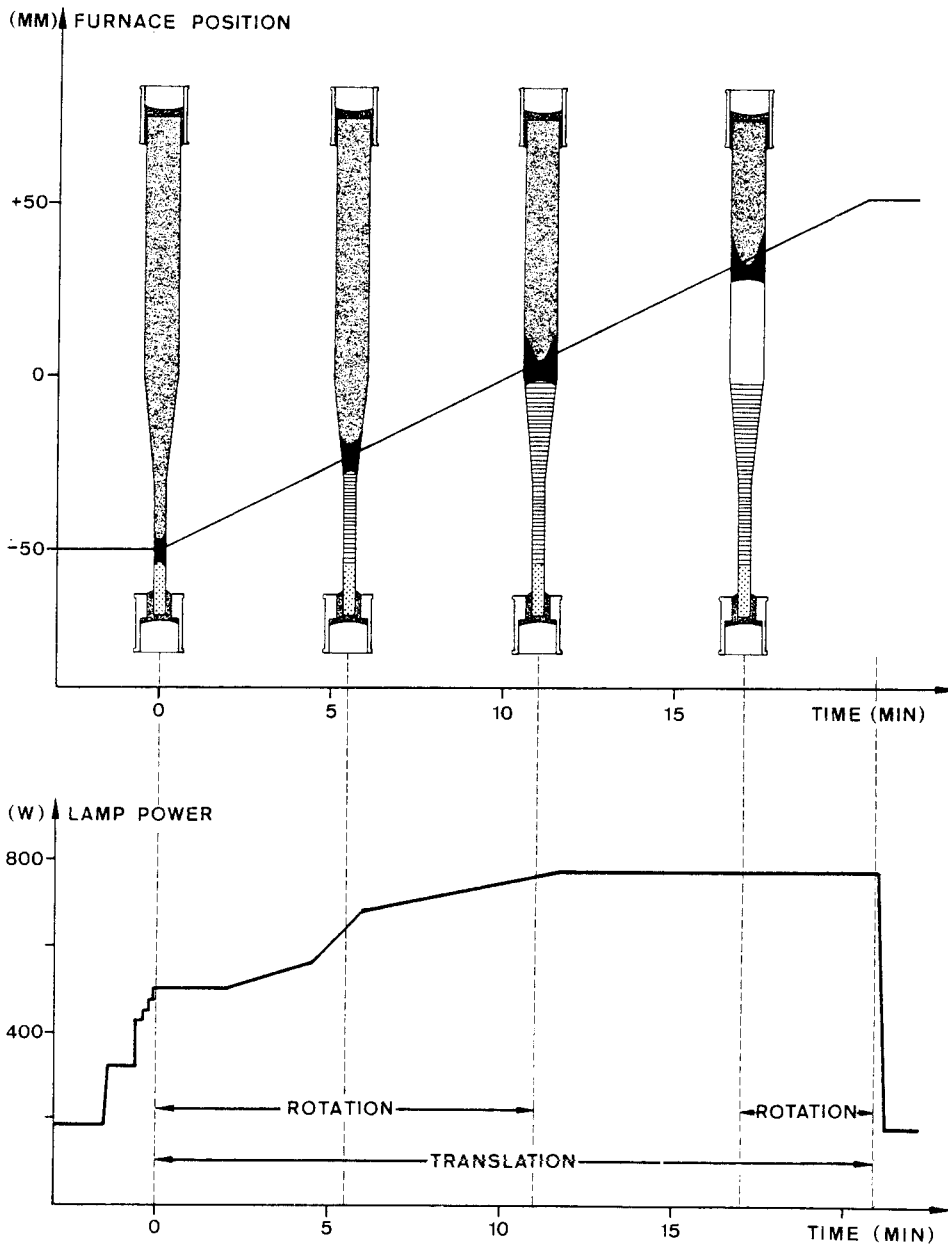


Fig. 2. Pulling and heating laws for Exp. 1-ES-321 aboard Spacelab-1.

gravity and surface tension always cause the melt to broaden at the lower end (so that the interface adopts an S-shape).

In space the situation is different. After establishing the liquid zone, its volume is, due to an 8%

decrease in volume of Si upon melting, too small to form a cylindrical bridge, let alone an outward bulging surface. As a consequence, the diameter of the growing crystal will initially decrease until the melt attains a meniscus angle of  $11^\circ$  (see fig. 4).

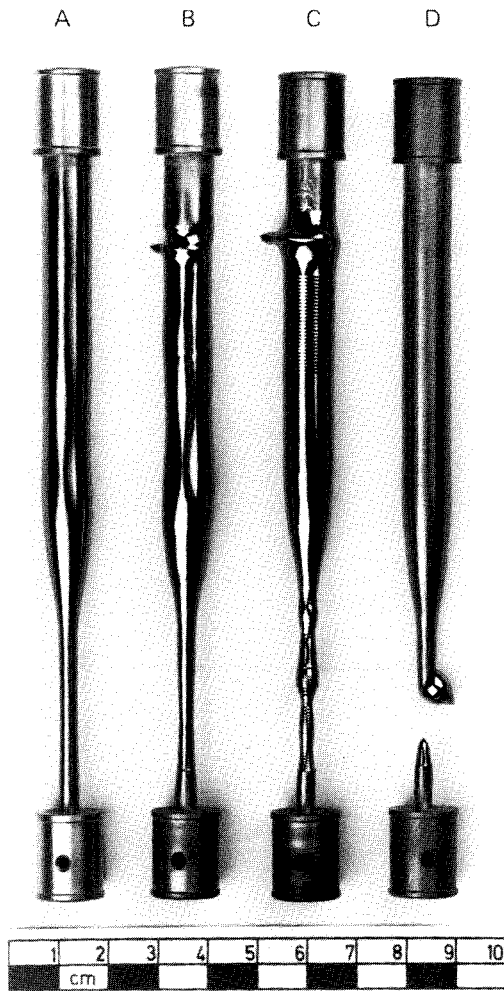


Fig. 3. Silicon rods: (A) unprocessed; (B) reference processed on ground; (C) sample successfully processed in flight; (D) sample processed in flight until bridge disruption occurred.

This diameter reduction tends to be less pronounced and would eventually recover, since in steady state growth the amount of material melting must equal the amount crystallizing.

But this transient decrease in diameter may affect the stability of the zone. The margin of stable zone lengths thus becomes even smaller in microgravity than on earth, and a very skillful experimentation is required to steer clear from zone disruption on the one hand and of solid/liquid interfaces touching on the other hand.

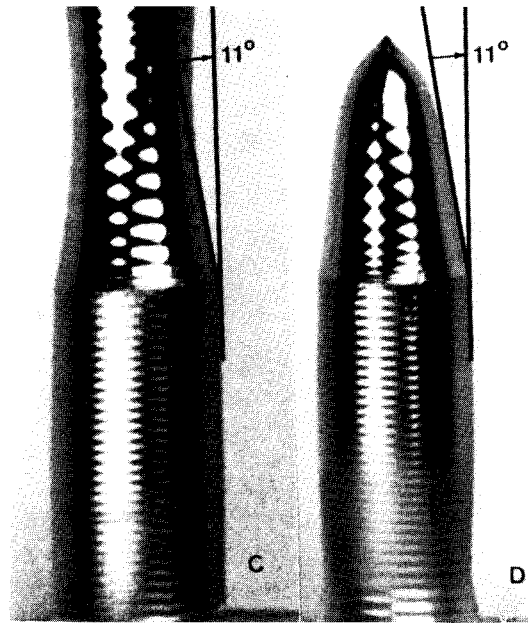


Fig. 4. Magnified view of the neck region for the two crystals processed in flight (figs. 3C and 3D) showing the growth angle at start.

Rotation of the end supports is normally imposed to uniformize the heating. For instance, the furnace used here produced a two-lobed non-axisymmetrical radiation pattern. Fortunately, the rotation rates in use were so low that the influence on outer shape and stability limit seems negligible. Most of the sample, however, was grown without rotation, suffering the asymmetry of the radiation pattern.

### 3. Experimental results

Two floating zone experiments were initiated during the Spacelab-1 mission. The first one took its scheduled course: a molten zone could be established in the neck and made to travel all the way to the end of the sample (fig. 3C). There was video recording aboard and, during most of the time, TV transmission to the ground. The sequence of outer shapes of the melt was gathered from the video tapes and correlated with the crystals grown from these melts (fig. 5). The irregularly shaped neck is the result of the difficulties

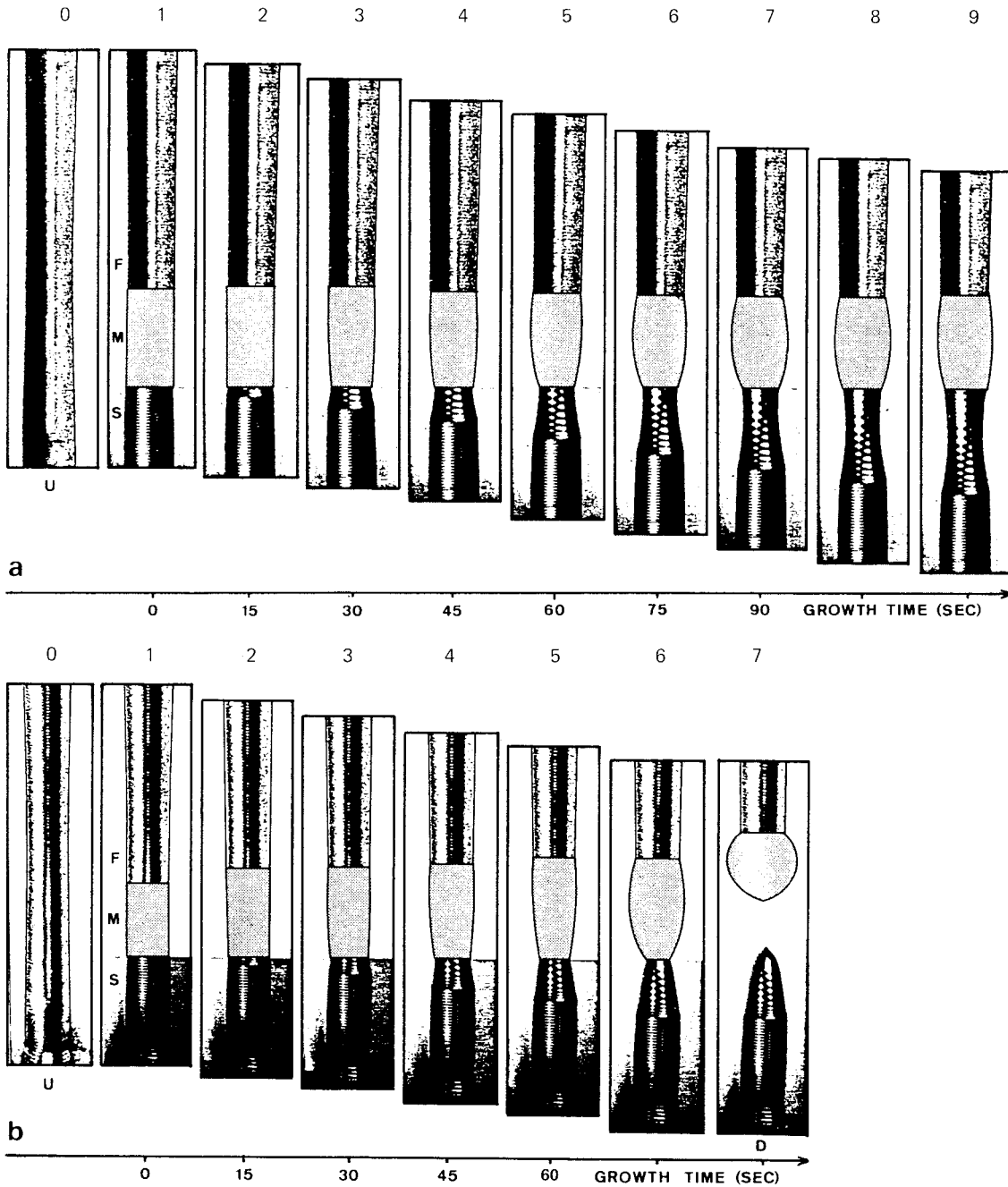


Fig. 5. Sequence of molten zones (depicted from video pictures): (a) successful growth (fig. 3C); (b) bridge disruption in the second trial. U unmolten crystal, S seed crystal, M melt, F feed crystal. Note that shape D in (b) immediately follows its previous picture; all others are 15 s apart.

encountered in adjusting by hand the proper zone length because of the meniscus problem mentioned above.

The second run had to be terminated shortly after starting of the zone travel because of rupture of the molten bridge (fig. 3D shows the two pieces

of that sample). Apparently, the zone length had become too large and the crystal diameter had decreased to such a degree that disruption near the lower interface occurred. The same occurrence had already taken place during a similar experiment in a sounding rocket [8].

A detailed view of the necks of the samples processed on board is presented in fig. 4. The rotation rims appearing on the surface show that the samples were being rotated during growth. Crystal perfection evaluation, as well as a comparison of the earth grown and space grown crystals, concerning crystal structure, defect concentration and dopant distribution, are reported elsewhere [5,6].

**4. Theoretical analysis**

What information can be gained by the experimenter with floating zones from the fluid-mechan-

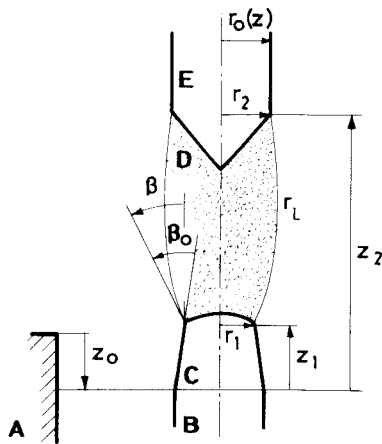


Fig. 6. Geometry and nomenclature used in the liquid bridge modeling of the floating zone growth: (A) furnace reference, (B) seed, (C) crystal grown, (D) melt, (E) feeding rod. All dimensions are scaled with seed radius \$r\_0(0)\$. Besides, the following parameters are introduced:

$$R = \frac{2r_L}{r_2 + r_1}, \quad H = \frac{r_2 - r_1}{r_2 + r_1},$$

$$\Lambda = \frac{z_2 - z_1}{r_2 + r_1}, \quad V = \frac{8\pi \int_{z_1}^{z_2} r_L^2 dz}{(r_2 + r_1)^3}.$$

anical theory of liquid bridges? For instance: Were the molten bridges equilibrium capillary menisci? How far were they from capillary instability? In all, what lessons from liquid bridge analysis can be advantageously used in crystal growth?

The fluid-mechanical behaviour of silicon floating zones can easily be explained by the simple liquid bridge theory of Laplace [9–16], provided the following simplifications are introduced:

- (a) Axisymmetric geometry.
- (b) Quasistatic configurations.
- (c) Constant material properties.
- (d) Negligible gravity, *g*-jitter and centrifugal effects.
- (e) Deep melting (molten core).
- (f) Free surface anchorage at both ends (seems to be quite realistic).

Under these hypotheses, the questions posed above may be answered as follows:

Molten free surfaces at equilibrium should be part of a constant mean curvature surface (Plateau surface). They can be determined from three non-dimensional parameters as, for instance, end diameter ratio *H* (see fig. 6 for nomenclature), length divided by mean diameter  $\Lambda$ , and straight volume

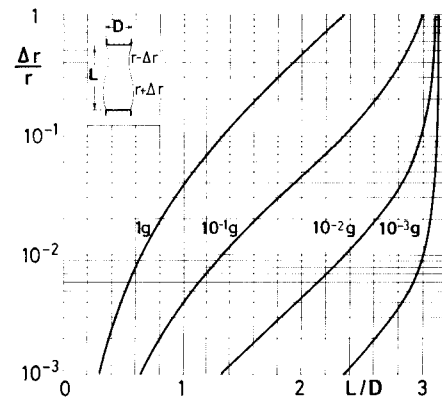


Fig. 7. Relative radial deformation in a cylindrical liquid bridge of radius 4 mm (\$\rho = 2520 \text{ kg/m}^3\$, \$\sigma = 0.75 \text{ N/m}\$) due to a residual axial gravity. It may be interpreted as the maximum allowable uncertainty to be able to detect distortions from equilibrium. In other words, the noise due to a \$10^{-3} \text{ g}\$ environment in a bridge with \$L/D = 3\$ imposes radial variations of 1% over the equilibrium cylinder. From another point of view, bridges with \$L/D = 1\$ will be distorted by only 4% on Earth.

$V$  (or neck or bulging ratio, which is easier to measure). Although an explicit expression may be developed for small deviations from the cylinder,

complicated graphical interpolation or involved computing are required in a general case. It should be noted, in any case, that in order to be able to detect deviations from equilibrium in real situations with small bridges (some millimetres in diameter), an accuracy of micrometres would be required. Present data analysis (manually digitized molten shapes from a TV screen) introduce an uncertainty of 5% in radii, much higher than the 0.1% required to detect perturbations of  $10^{-3}$  g, for instance, as explained in fig. 7.

Once the three nondimensional parameters that determine the shape are measured, it is easy to look at the stability diagram for liquid bridges anchored to unequal discs [13] and (see fig. 8) to find how far the stability limit is, with respect to the parameters mentioned above. However, from a practical point of view, what matters is the stability limits with respect to the directly controlled inputs: furnace power and pulling laws, which is a much more involved task.

The main lesson from liquid bridge theory is that the sequence of molten shapes during growth can be predicted as a function of the position of the fronts and, if the small difference in density is accounted for, of the volume of immersed solid tips. Thus, if a thermal analysis of furnace and rod could model these three parameters as functions of the heating and pulling laws, the behaviour of the floating zone should be entirely predictable and, consequently, programmed to a better advantage.

**5. Liquid bridge modeling**

The geometry used is sketched in fig. 6. All dimensions are scaled with the radius of the first resolidified rod section. If, for the sake of clarity, the difference between the density of liquid and solid silicon (the latter 8% larger) is neglected, the sequence of molten shapes during growth  $r_L(z, t)$  is determined by knowing the initial rod shape  $r_0(z)$  and the movement of the fronts:  $z_1(t)$  and  $z_2(t)$ .

The procedure is as follows. From initial conditions, the liquid free surface is known. From that, resolidification should proceed with a constant

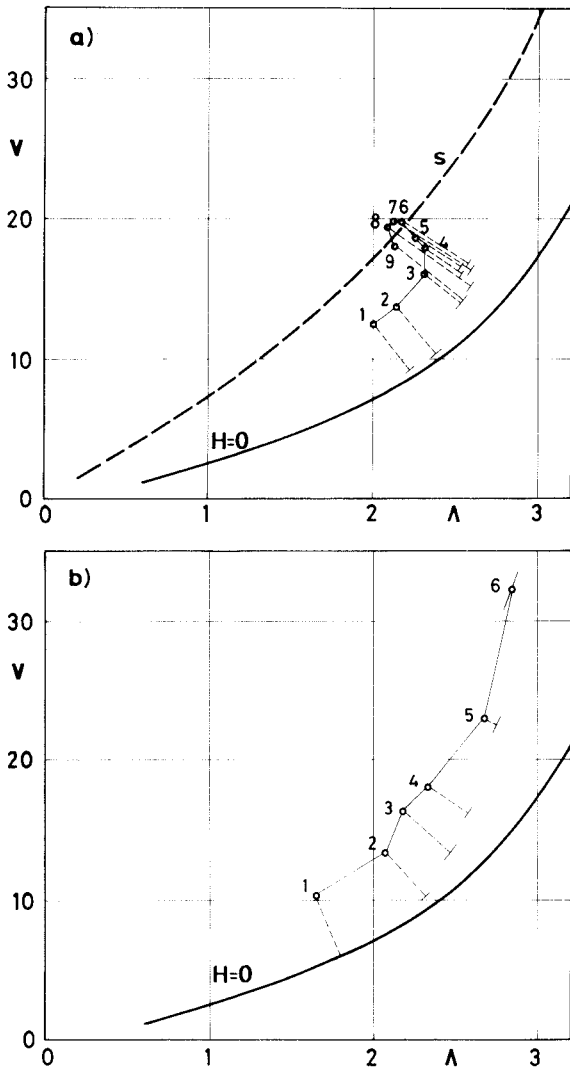


Fig. 8. Capillary stability diagram for a molten bridge. The points correspond to shapes in fig. 5. Dashed lines indicate the stability margin (minimum distance to the stability boundary in the slenderness–volume diagram [13]). (a) Stable growth. It is seen that after shapes 3 and 4 the zone gets away from the unstable limit, approaching a point in curve  $s$  which is the loci of cylindrical growth configurations for silicon (a barrel-shaped molten zone with  $11^\circ$  of bulging that moves along a cylindrical rod). (b) Growth with bridge disruption. It is seen how the last shape in fig. 5b was unstable (because of the smallness of the sample, 3.8 mm of diameter, the breaking is instantaneous).

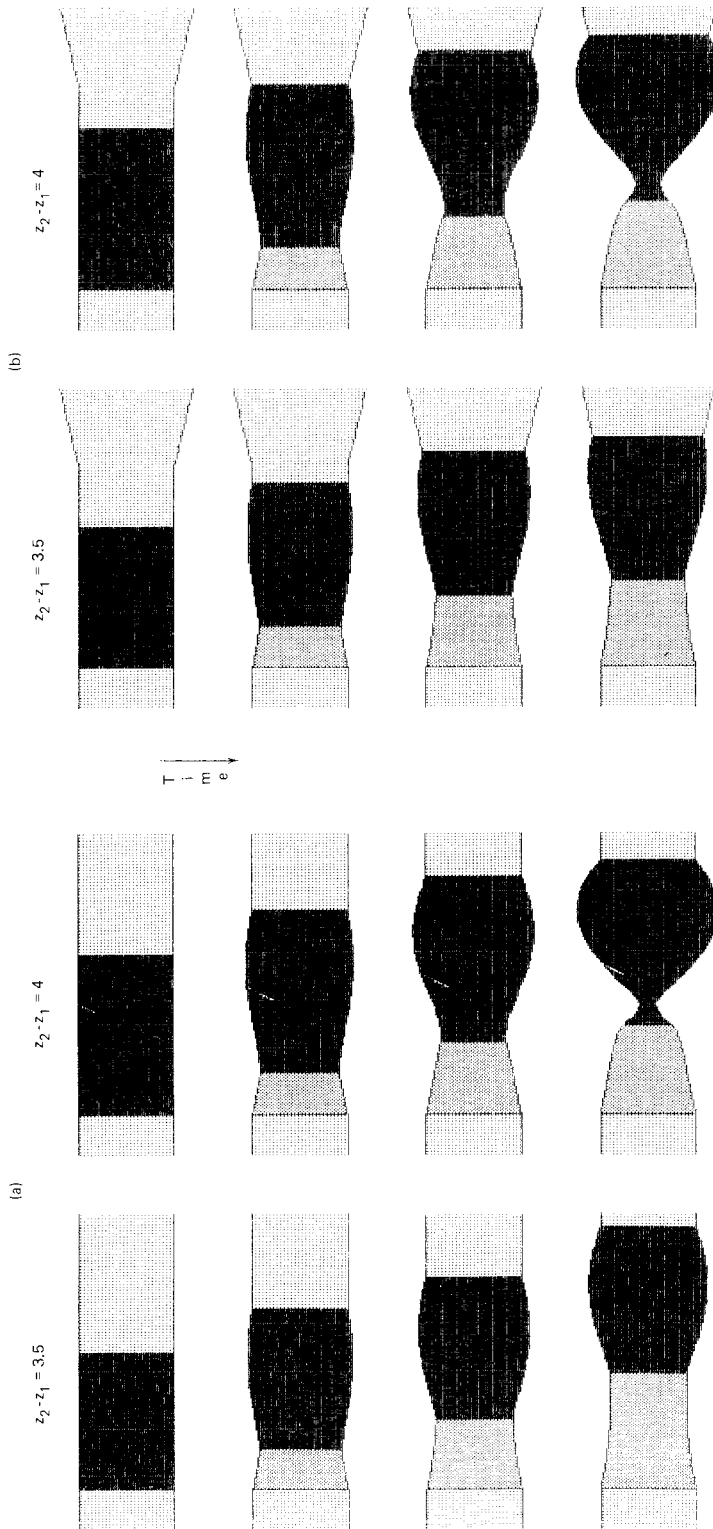


Fig. 9. Example of predicted evolution of the solidification radius,  $r_L$ , with distance from the seed,  $z$ , during floating zone processing of a silicon rod of initial shape  $r_0(z)$ . In this example, the external length of the molten bridge,  $z_2 - z_1$ , is assumed constant with time. Note that, in both cases shown, if  $z_2 - z_1 = 3.5$  the crystal grows trying to recover the initial shape, whereas if  $z_2 - z_1 = 4$  the growing gets unstable and the bridge breaks. (a) Initially cylindrical rod. (b) Initially shaped as a cylinder-cone joint.

receding angle of  $\beta_0 = 11^\circ$  from the liquid free surface, thus diminishing the solidification radius and displacing some volume  $v_{\text{dis}}$  from the initial rod towards the molten bridge (ahead of the solidification front). The liquid bridge then tends to get a barrel shape and thus, if it does not gets destabilized in the way, the angle at the border will increase restoring the solidification front radius to that of the original rod. In mathematical form:

$$dz_1/dt = f_1(t), \tag{1a}$$

$$dz_2/dt = f_2(t), \tag{1b}$$

$$dr_1/dt = (dz_1/dt) \tan(\beta - \beta_0), \tag{1c}$$

$$dv_{\text{dis}}/dt = \pi [r_0^2(z_1) - r_1^2] dz_1/dt, \tag{1d}$$

which can easily be integrated with a standard Runge–Kutta routine, once the initial conditions  $z_1 = 0, z_2 = z_2(0), r_1 = r_1(0) = r_0(0), v_{\text{dis}} = 0$  are fixed, and  $\beta$  is expressed as a function of the variables, as explained below.

To this aim, a further simplification is now introduced: the liquid bridge shape is assume not to deviate too much from a cylinder so that the handy linear approximation

$$R^2(Z, H, \Lambda, V) = 1 + \frac{V - 2\pi\Lambda}{2\pi\Lambda} \frac{\cos Z - \cos \Lambda}{\Lambda^{-1} \sin \Lambda - \cos \Lambda} + 2H \frac{\sin Z}{\sin \Lambda} + H^2 \frac{\Lambda^{-1} \sin \Lambda - \cos Z}{\Lambda^{-1} \sin \Lambda - \cos \Lambda}, \tag{2}$$

is valid. Here, a local scale is used for the shape such that it goes from  $-\Lambda$  to  $+\Lambda$ , with  $R(-\Lambda) = 1 - H, R(+\Lambda) = 1 + H, \Lambda$  being the slenderness, and

$$V = \int_{-\Lambda}^{\Lambda} \pi R^2 dZ$$

the straight volume between ends (including immersed solid tips). These local parameters are related to the growth ones by

$$H = [r_0(z_2) - r_1] / [r_0(z_2) + r_1], \tag{3a}$$

$$\Lambda = (z_2 - z_1) / [r_0(z_2) + r_1], \tag{3b}$$

$$V = 8 \frac{v_{\text{dis}} + v_0(z_2) - v_0(z_1)}{[r_0(z_2) + r_1]^3}, \tag{3c}$$

where  $v_0(z)$  is the volume of the initial rod  $r_0(z)$  from 0 to  $z$ . Furthermore,  $\beta_0 = 11^\circ$  and, within the linear approximation above,  $\beta$  is directly given by

$$\beta = \arctan \left\{ \left[ \frac{2H}{\tan \Lambda} + \frac{V/2\pi\Lambda - 1 - H^2}{1/\Lambda + 1/\tan \Lambda} \right] \times [2(1 - H)]^{-1} \right\}. \tag{4}$$

For a given furnace and initial rod, the value  $z_2(t=0)$  and the two functions  $f_1(t)$  and  $f_2(t)$  only depend on the heating and pulling laws imposed. Further work will be needed to build this thermal model, but the simple procedure detailed above allows one to gain much insight in the behaviour of floating zones processing. To that aim, simple trials can be run and the effects observed. Fig. 9 presents the results of such a trial: the distance between solidification and melting fronts has been assumed constant and its influence on the stability of growing studied (similarly, other laws such as maintaining the molten volume, or the free surface area, etc., can be exercised). As shown in fig. 9, different initial rod geometries can be easily studied.

The general procedure is implemented in a computer program that works as follows:

- (1) Read silicon data (solidification angle, liquid and solid density, melting temperature, specific heats, enthalpy of fusion, thermal conductivities, etc).
- (2) Read initial rod data (section profile for an axisymmetric rod).
- (3) Read experiment data (pulling and heating laws as functions of time  $t$ ).
- (4) Compute molten bridge base parameters (position of solid/melt fronts and solid volume immersed inside the straight volume, as functions of time) either from real experiments or from a thermal model (still lacking).
- (5) Compute liquid bridge base parameters  $H(t), \Lambda(t)$  and  $V(t)$  from their definitions.
- (6) Compute liquid bridge shape from base parameters by using a liquid bridge model (eq. (2)).
- (7) Show predicted molten-zone evolution for the data given.

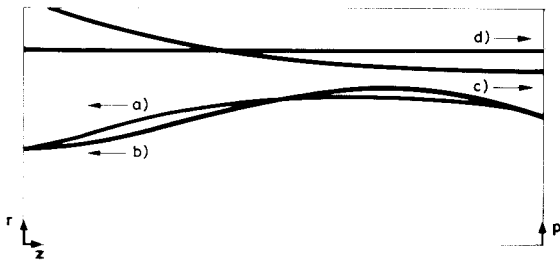


Fig. 10. Experimental (a) and theoretically predicted (b) shapes corresponding to stage 6 in fig. 5b. Melt shape (after a video recording of the actual growth) appears more flattened than predicted. Its pressure profile (c) should be uniform as for the theoretical shape (d) (assuming constant surface tension) and it is clearly not.

(8) If real experiment sequence available, compare molten shapes with predictions. In fact, this is the case here, and fig. 10 shows the comparison for shape 6 in fig. 5b.

## 6. Conclusions

A straightforward analysis of results from Exp. 321 on silicon crystal growth by the floating zone technique is made, from the fluid-mechanical point of view, assuming constant surface tension and no force field applied. The main results may be summarized as follows:

- (1) The stable evolution that occurred in the first trial of Exp. 321 is accurately predicted by the model (fig. 8a).
- (2) The unstable evolution that occurred in the second trial of Exp. 321 is accounted for and accurately predicted by the model (fig. 8b).
- (3) Uncertainty in shape discrimination, due to smallness of the sample, prevents a finer analysis

of disturbances upon the equilibrium configurations (fig. 7).

(4) Real bridges appear to be more flattened than expected (fig. 10). Sizable departures of a constant pressure profile from observed shapes (pressure diminish towards the neck) need further explanation (maybe nonuniform surface tension due to temperature gradients).

(5) From the history described above, the sequence of shapes may be computed, thus, the next step should be to model the thermal problem to be able to predict the sequence of shapes from the heating and pulling laws.

## References

- [1] A. Eyer, R. Nitsche and H. Zimmermann, *J. Crystal Growth* 47 (1979) 219.
- [2] A. Eyer, B.D. Kolbesen and R. Nitsche, *J. Crystal Growth* 57 (1982) 145.
- [3] R. Schoenholz, R. Dian and R. Nitsche, *J. Crystal Growth* 72 (1985) 72.
- [4] G. Nagel and K.W. Benz, *Advan. Space Res.* 4.5 (1984) 23.
- [5] A. Eyer, H. Leiste and R. Nitsche, *ESA SP-22* (1984) 173.
- [6] A. Eyer, H. Leiste and R. Nitsche, *J. Crystal Growth*, submitted.
- [7] T. Surek and B. Chalmers, *J. Crystal Growth* 29 (1975) 1.
- [8] A. Eyer, H. Leiste and R. Nitsche, *J. Crystal Growth* 71 (1985) 173.
- [9] I. Martinez, *COSPAR Space Res.* 18 (1978) 519.
- [10] I. Da Riva and I. Martinez, *ESA SP-142* (1979) 67.
- [11] I. Martinez and D. Rivas, *Acta Astronautica* 9 (1982) 339.
- [12] A. Sanz and I. Martinez, *J. Colloid Interface Sci.* 93 (1983) 235.
- [13] I. Martinez, *ESA SP-191* (1983) 267.
- [14] J. Meseguer, *J. Crystal Growth* 67 (1984) 141.
- [15] J. Meseguer, *ESA SP-222* (1984) 297.
- [16] I. Martinez, *ESA SP-222* (1984) 31.